energies

MDPI

Article

Molecular Investigation on the Displacement Characteristics of CH_4 by CO_2, N_2 and Their Mixture in a Composite Shale Model

Liang Gong, Yuan Zhang, Na Li, Ze-Kai Gu, Bin Ding and Chuan-Yong Zhu *

College of New Energy, China University of Petroleum (East China), Qingdao 266580, China; lgong@upc.edu.cn (L.G.); z18060014@s.upc.edu.cn (Y.Z.); b19150002@s.upc.edu.cn (N.L.); s19150032@s.upc.edu.cn (Z.-K.G.); dingbin@upc.edu.cn (B.D.)
* Correspondence: cyzhu@upc.edu.cn

Abstract: The rapid growth in energy consumption and environmental pollution have greatly stimulated the exploration and utilization of shale gas. The injection of gases such as CO_2, N_2, and their mixture is currently regarded as one of the most effective ways to enhance gas recovery from shale reservoirs. In this study, molecular simulations were conducted on a kaolinite–kerogen IID composite shale matrix to explore the displacement characteristics of CH_4 using different injection gases, including CO_2, N_2, and their mixture. The results show that when the injection pressure was lower than 10 MPa, increasing the injection pressure improved the displacement capacity of CH_4 by CO_2. Correspondingly, an increase of formation temperature also increased the displacement efficiency of CH_4, but an increase of pore size slightly increased this displacement efficiency. Moreover, it was found that when the proportion of CO_2 and N_2 was 1:1, the displacement efficiency of CH_4 was the highest, which proved that the simultaneous injection of CO_2 and N_2 had a synergistic effect on shale gas production. The results of this paper will provide guidance and reference for the displacement exploitation of shale gas by injection gases.

Keywords: composite shale model; displacement; molecular simulations; shale gas; injection gases

Citation: Gong, L.; Zhang, Y.; Li, N.; Gu, Z.; Ding, B.; Zhu, C. Molecular Investigation on the Displacement Characteristics of CH_4 by CO_2, N_2 and their Mixture in a Composite Shale Model. *Energies* **2021**, *14*, 2. https://dx.doi.org/10.3390/en14010002

Received: 26 November 2020
Accepted: 17 December 2020
Published: 22 December 2020

1. Introduction

The consumption of traditional energy such as oil and coal induces increasingly severe environmental pollution and the greenhouse effect. Therefore, it is urgent to improve the energy consumption structure and reduce the consumption of oil and coal. The environmental pollution and greenhouse gas emission problems can be alleviated once traditional energy is replaced by shale gas, which is a type of clean low-carbon energy [1,2]. The main component of shale gas is methane (CH_4), which is generally stored in a shale reservoir in three states (i.e., adsorbed state, free state, and dissolved state) [3]. Among them, CH_4 with an adsorbed state plays a dominant role [4]. Therefore, transforming adsorbed-state CH_4 to a free state is the critical process in shale gas exploitation. Unfortunately, the low porosity and permeability of shale reservoirs significantly inhibit the desorption and diffusion processes of adsorbed CH_4 molecules, increasing the difficulty of shale gas recovery.

Currently, hydraulic fracturing is the most commonly used method to improve the productivity of shale gas recovery by dramatically enhancing the shale porosity and permeability [5]. However, this method faces the shortcomings of waste production and water pollution [6,7]. By contrast, these disadvantages could be avoided by replacing water with supercritical carbon dioxide (CO_2) during the fracturing process. Apart from this, injecting CO_2 into shale reservoirs as a means of reducing greenhouse gas emissions is regarded as one of the promising strategies for CO_2 sequestration. Thus, the use of CO_2 as an alternative fluid to enhance shale gas recovery has attracted increasing attention and has recently stimulated many research efforts [8–11]. Nitrogen has proved to be another potential fracturing fluid for efficiently enhancing shale gas recovery, owing to its low viscosity and price [4,12,13]. Meanwhile, experiments conducted by the authors of [14]

revealed that CO_2-N_2 mixed gas injection exhibits improved shale gas recovery performance compared to CO_2 injection alone. Therefore, an understanding of the displacement behaviors between CH_4 and CO_2, N_2, and the mixture of CO_2-N_2, from a micro-scale perspective, is immensely valuable in guiding the efficiency of shale gas recovery and CO_2 sequestration.

Many efforts by different research groups have been devoted to the experimental investigation of the effects of injection gases on shale gas recovery [15,16]. For instance, nuclear magnetic resonance (NMR) was adopted by the authors of [17] to explore the effect of CO_2 pressure on the efficiency of shale gas recovery. Their results indicated that the desorption efficiency of the adsorbed CH_4 was improved by 27% and 26% when the CO_2 was kept at ambient pressure and abandonment pressure, respectively. Moreover, the effects of shale reservoir temperature, pressure, and particle size, CO_2 flow rate, and pressure on the efficiency of shale gas recovery were studied in [18]. They found that a high injection pressure of CO_2 had the benefit of enhancing the efficiency of shale gas recovery, whereas the effects of CO_2 flow rate and shale reservoir temperature could be ignored. Furthermore, the effect of gas injection composition, including CO_2, N_2, and CO_2-N_2 mixed gas, on the efficiency of shale gas recovery were investigated in [19–21]. In summary, the presence of N_2 has the benefit of prolonging the breakthrough time of CO_2 and achieving the goal of CO_2 storage over the long term, and the ratio of CO_2/N_2 is an important parameter for optimizing shale gas recovery and CO_2 storage. Although many scholars [17,19] tried to experimentally reveal the displacement mechanism between the injection gases and CH_4, a microscopic mechanism has not yet been reported due to the limitations of measurement techniques.

As alternatives, molecular simulation methods, including density functional theory (DFT), grand canonical Monte Carlo (GCMC), and molecular dynamics (MD), are effective approaches to explore the interactional characteristics between the gases and shale reservoirs as well as the displacement behaviors between injection gases and CH_4 [22]. For instance, the authors of [23] proved that the adsorption energy of CO_2 was much larger than that of CH_4 using a DFT model. The authors of [24] indicated that the van der Waals' force plays a dominant role in the interactions between CH_4 and the kerogen surface. In [25], the authors explored the competitive adsorption behavior between CO_2 and CH_4 using a GCMC model. Their results indicated that the adsorption capacity of CO_2 was much higher than that of CH_4 under various conditions. Similarly, the authors of [26,27] investigated the effect of pore size on the adsorption behaviors of CH_4 in kaolinite and quartz, respectively, using the GCMC mothed. They found that the adsorption performance of the shale matrix on CH_4 was exponentially reduced with an increase in pore size. The authors of [28] studied the diffusion characteristics of CH_4 and CO_2 in the shale matrix based on MD. Their results showed that the diffusion coefficient of CH_4 and CO_2 in nanoscale pores of the montmorillonite slit decreased with increasing pressure, and the diffusion coefficient of CH_4 was larger than that of CO_2.

Moreover, the authors of [29] proved that the displacement performance of CH_4 decreased gradually once CO_2, N_2, and H_2O were successively injected in carbon nanotubes. In [30], the authors investigated the displacement of shale gas by CO_2 and the sequestration of CO_2 simultaneously in a shale matrix at different geological depths using the GCMC method. They pointed out that pore size played a significant role in the displacement of CH_4 by CO_2, and the optimum geological depth for the displacement of CH_4 by CO_2 was about 1.0 km. Besides, the authors of [4] used the MD method to simulate the displacement process of CH_4 by CO_2 and N_2 in a composite model of quartz and methylnaphthalene. They found that the displacement efficiency of a small pore (30 Å) was the highest and the displacement efficiencies of CH_4 by different gases were larger than 50% when the injection pressure was greater than 30 MPa. Although extensive studies on the displacement characteristics of CH_4 by single-component gas (CO_2, N_2, and H_2O) in various shale models were conducted, limited studies have been performed to explore the mechanism of shale gas displacement by mixed gas CO_2-N_2 from a microscopic perspective. The synergistic

effect of the simultaneous injection of N_2 and CO_2 on the displacement efficiency of CH_4 was observed experimentally [19], while the microscale mechanism of this phenomenon has not been made clear yet, and few studies have tried to explore it from the molecular level. Besides, the optimal N_2/CO_2 ratio at which the displacement efficiency reaches its maximum has not been reported. However, this value was regarded as one of the most important parameters to enhance shale gas recovery. On the other hand, thorough research on the displacement process of CH_4 in a realistic organic–inorganic composite shale model under a complex environment, such as a humid environment, is still lacking.

2. Numerical Model and Methodology

2.1. Model Description

In this study, a composite shale model consisting of two inorganic layers (kaolinite) and two organic layers (kerogen IID, which belongs to the over-mature stage of kerogen II), as shown in Figure 1, was established for numerical simulations. The reason for choosing the kaolinite and kerogen IID as the inorganic and organic layers, respectively, was that these two materials are the typical components of actual shale. This composite shale model establishment process can be described as follows:

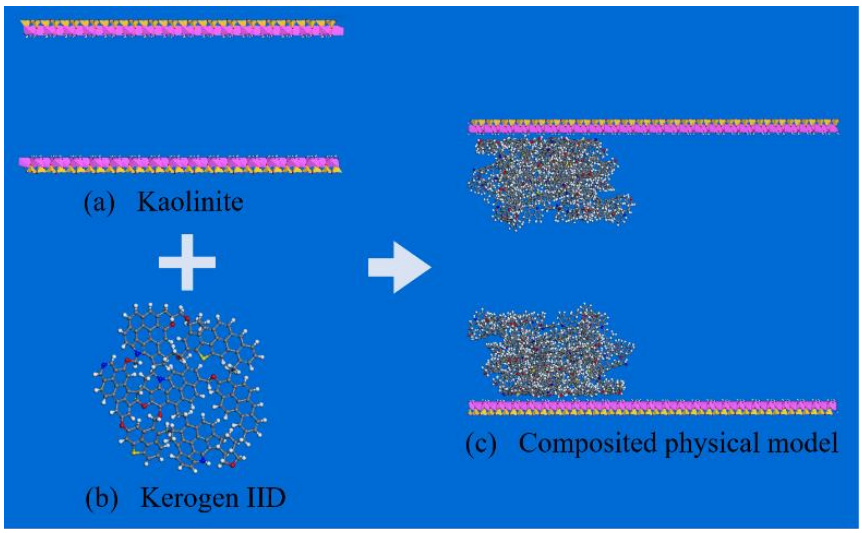

Figure 1. The composite shale model of kaolinite and kerogen IID.

(1) The inorganic kaolinite layered model box was first established as shown in Figure 1a, in which the parameters of the kaolinite cell structure were obtained from the data in [31];
(2) A single kerogen IID molecule was built based on the data from [32] (Figure 1b), and then the corresponding kerogen IID box with 11 kerogen IID molecules was established according to the size of the layered inorganic mineral lattice;
(3) The kaolinite box in Figure 1a and two kerogen IID boxes were combined to form a composite shale model (Figure 1c).

Density is one of the most important physical properties of organic materials. Figure 2 shows the density of the present kerogen IID box as a function of a relaxation time. It can be seen that when the density of the kerogen IID box reached stability, its average value was about 1.28 g/cm^3, which is in good agreement with the value of 1.1 g/cm^3–1.4 g/cm^3 for kerogen IID in real shale reservoirs [33], indicating the this kerogen IID model is reliable. The adsorption process of CH_4 in kerogen boxes at T = 338 K was also conducted, and the calculated adsorption isotherm was compared with that in [34], as shown in Figure 3. The compared result in Figure 3 further validates the present kerogen IID box model and shows the reliability of the adsorption model used in the present paper.

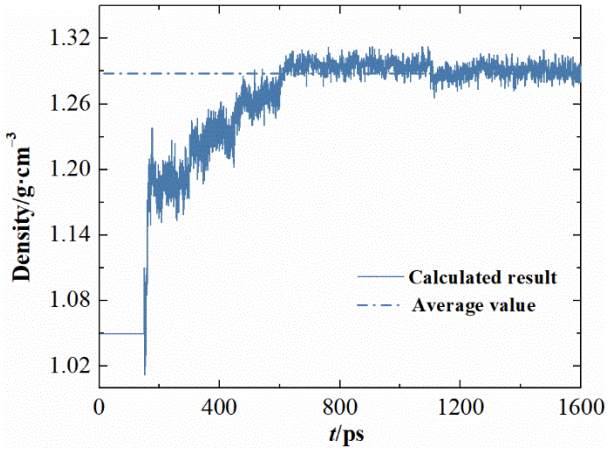

Figure 2. The density of the kerogen box.

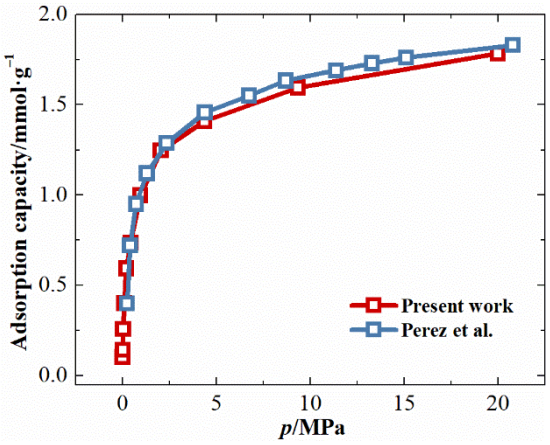

Figure 3. Adsorption isotherm of the kerogen box [34].

Once the composite shale matrix model (Figure 1c) was established, CH_4 was pre-adsorbed on this model at a certain temperature and pressure using the GCMC method, as shown in Figure 4. The red region on the left side of the composite shale model is the injection gas, which could be CO_2, N_2, or CO_2-N_2 mixed gas.

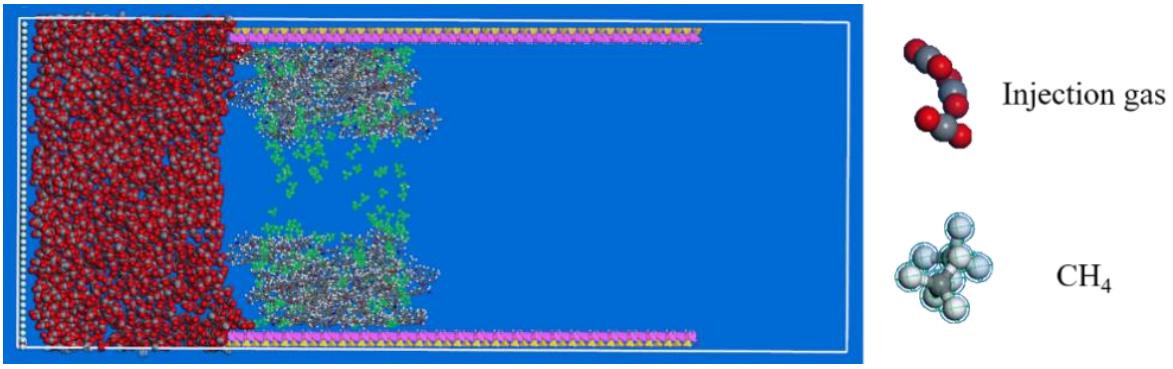

Figure 4. The physical model for the shale gas displacement process.

2.2. Simulation Details

In this study, the GCMC method was adopted to simulate the adsorption process of CH_4 in the above composite model. In the GCMC simulations, the van der Waals interaction and electrostatic interaction between molecules were calculated by the Atom and Ewald summation methods, respectively. The adsorption equilibrium and adsorption production of CH_4 were set as 5×10^6 and 1×10^7, respectively. We used the condensed-phase optimized molecular potentials for atomistic simulation studies (COMPASS) force field, which can effectively simulate molecular systems including organic polymers and inorganic molecules, and the non-bond cutoff radius was set as 1.9 nm. After obtaining the pre-adsorption configuration of CH_4 in the composite shale model (Figure 4), the MD method was employed to investigate the displacement characteristics of CH_4 under different conditions. The force field parameters and interaction parameters used in the MD simulations were set as those in the above GCMC method. The canonical ensemble (NVT) and a Nose–Hoover thermostat were used to control the temperature, and the total calculation time was set as 1.0 ns with the time step of 1.0 fs.

To evaluate the displacement capacity efficiency of CH_4 by the injection gas, the displacement efficiency R_{dis} is defined as follows:

$$R_{dis} = (N_{ad} - N_{dis})/N_{ad} \quad (1)$$

where N_{ad} $(\text{mmol}\cdot\text{g}^{-1})$ is the amount of pre-adsorbed CH_4 in the composite model, and N_{dis} $(\text{mmol}\cdot\text{g}^{-1})$ is the residual amount of CH_4 in the composite shale after the displacement process.

3. Results and Discussion

As mentioned in the introduction, there are many factors, including formation conditions and gas species, that influence shale gas displacement efficiency. Thus, in the following sections, different physical models with different pore size and water content are presented. Then, the influence of different factors, such as the formation temperature, pressure, pore size, gas composition, and water content, on the displacement characteristics and displacement efficiency of CH_4 is discussed.

3.1. The Influence of Pressure on the Displacement Characteristics

In order to examine the influence of gas pressure on the displacement characteristics of CH_4, the displacement processes of CH_4 by CO_2 at different pressures, including p = 6, 10, 15, 20 MPa, were investigated. Figure 5 plots the displacement capacity of CH_4 as a function of time under different pressures. In the figure, when the displacement process reaches a steady-state, the displacement capacity increases with the increase in the injection pressure. However, the growth rate of the displacement capacity gradually slows down with the increase in pressure (Figure 5b), which indicates that properly increasing the injection pressure is beneficial to the displacement of CH_4.

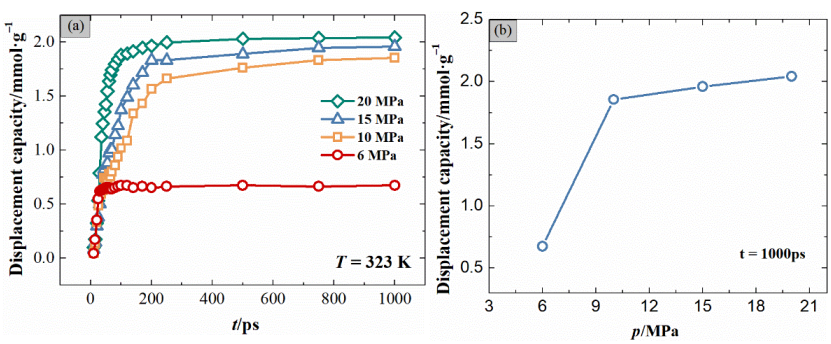

Figure 5. The displacement capacity of CH_4 by CO_2 (**a**) displacement capacity at different pressures; (**b**) displacement capacity as a function of pressure.

Figure 6 shows the displacement process with p = 20 MPa and T = 323 K at different times. The figure indicates that as time goes by, the CO_2 molecules on the left side gradually enter the slit and are gradually absorbed in the pores and the surface of the kerogen matrix. CO_2 molecules occupy the adsorption sites of CH_4, and the adsorbed CH_4 molecules are replaced from the shale reservoir. Then, the free-state CO_2 molecules displace the desorbed CH_4 molecules from the nanoscale pores.

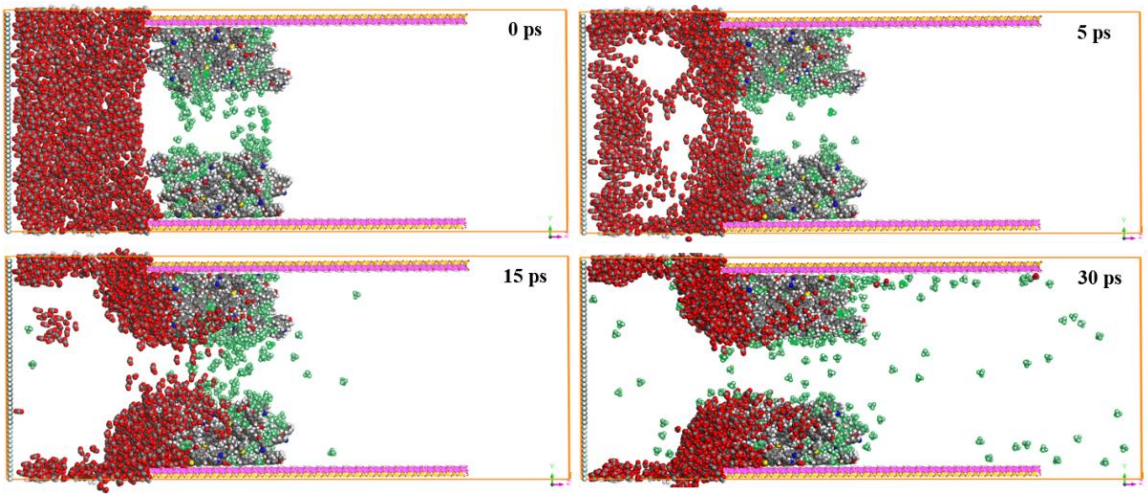

Figure 6. The displacement process of CH_4 by CO_2 with p = 20 MPa and T = 323 K.

Figure 7 plots the displacement efficiency as a function of pressure. It can be seen that as the injection pressure increases from 6 MPa to 10 MPa, the displacement efficiency increases by 44.4%. However, when the injection pressure is larger than 10 MPa, the increasing tendency of the displacement slows down. The displacement efficiency only increases by 7.0%, as the pressure increases from 10 MPa to 20 MPa. That means a further increase in the injection pressure is of little significance for enhancing shale gas recovery.

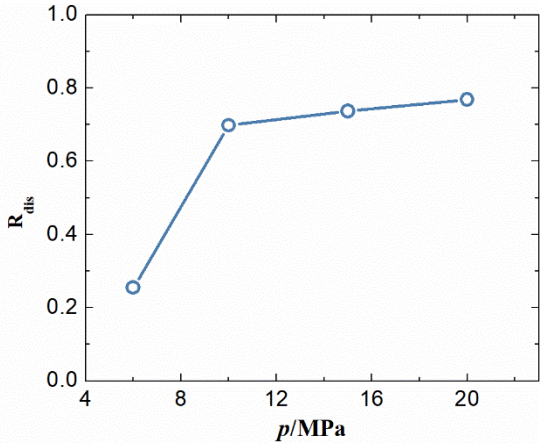

Figure 7. The displacement efficiency of CH_4 along with the injection pressure.

3.2. The Influence of Temperature on the Displacement Characteristics

Figure 8 plots the displacement capacity of CH_4 by CO_2 at different temperatures under p = 20 MPa, as a function of time. It can be seen that, as time goes by, the displacement capacity of CH_4 at higher temperatures climbs faster, and a higher temperature ultimately leads to a greater displacement capacity. This is because the activity of gas molecules increases with the increase in temperature. From Figure 9, it can be seen that with the same pore size of d = 2 nm, when the displacement process achieves a steady-state, and as the temperature of the reservoir increases from 298 K to 383 K, the displacement capacity of

CH_4 increases by 9.4%. Interestingly, when the injection temperature is low (T < 353 K), the displacement capacity increases linearly as temperature increases; however, as the injection temperature further increases, the increase of the displacement capacity is not obvious. Besides, Figure 10 shows that as the temperature increases, the displacement efficiency increases monotonously, indicating that increasing the injection or formation temperature is beneficial to the exploitation of shale gas.

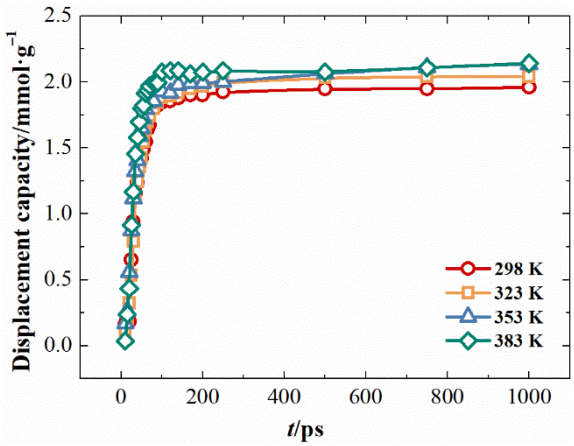

Figure 8. Displacement capacity of CH_4 by CO_2 at different temperatures over time.

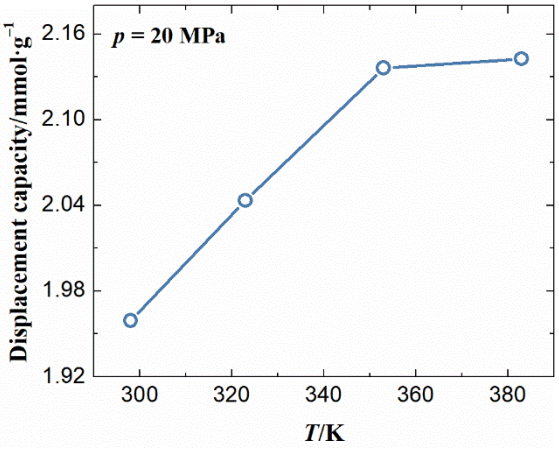

Figure 9. The terminal displacement capacity of CH_4 by CO_2 as a function of temperature.

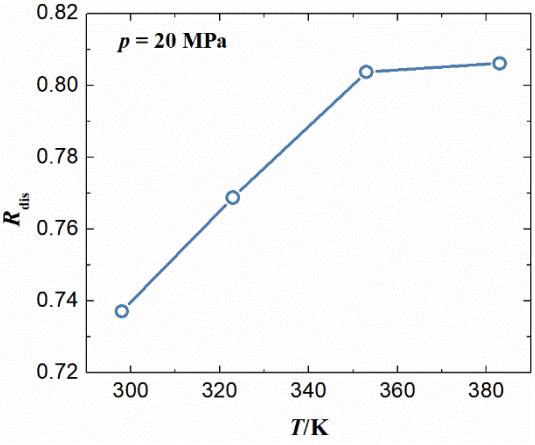

Figure 10. Displacement efficiency of CH_4 by CO_2 as a function of temperature.

3.3. The Influence of Pore Size on the Displacement Characteristics

Figure 11 plots the displacement capacity of CH_4 by CO_2 as a function of pore size. It can be seen that at the early stage of the displacement process, the displacement capacity in different pores increases sharply as time increases. In addition, as the pores size increases, the time required to reach steady-state decreases. This is because the larger pore size is conducive to the replacement of adsorbed CH_4 from the reservoir and is also beneficial to the diffusion of CH_4 in nanoscale pores. When the pore size increases from 1 nm to 3 nm, the displacement capacity increases by 11.8%. Figure 12 presents the displacement efficiency of CH_4 as a function of the aperture. When the pore size increases from 1 nm to 3 nm, the displacement efficiency only increases by 2.6%, which is smaller than the increment of the displacement capacity. This can be attributed to the fact that the pre-adsorbed CH_4 in larger pores is relatively larger than that in smaller pores.

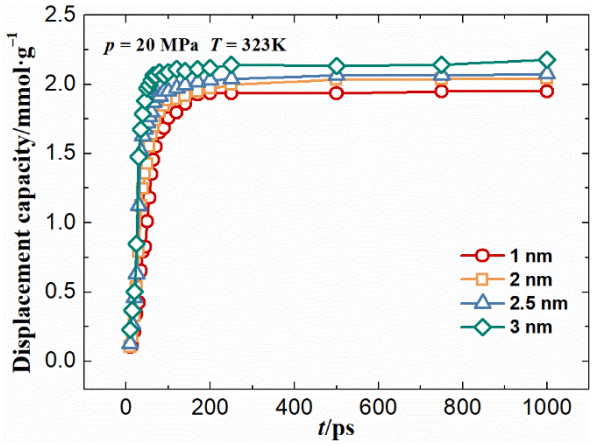

Figure 11. Displacement capacity of CH_4 by CO_2 with different pore sizes.

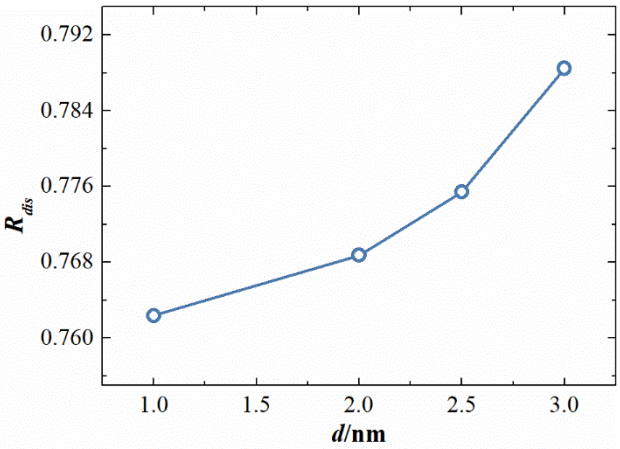

Figure 12. Displacement efficiency of CH_4 by CO_2 in different pore sizes.

3.4. The Influence of Gas Proportion on the Displacement Characteristics

Figure 13 shows the displacement capacity of CH_4 by gas with different proportions over time. It shows that at the early stage of the displacement process, the higher the nitrogen content, the larger amount of CH_4 that is displaced from the composite shale reservoir. This is because compared with CO_2, N_2 is not easily adsorbed on the composite shale reservoir (Figure 14), and the free-state N_2 can displace CH_4 from the shale pores in the early stage of the process. Moreover, the free-state N_2 can also reduce the partial pressure of CH_4 in the shale pores and promote the self-desorption process of CH_4. From Figure 15, it can be seen that when the displacement process reaches a steady-state, the dis-

placement capacity of CH_4 by N_2 is the least. This is because the adsorption capacity of the shale reservoir to nitrogen is slightly lower, and thus the amount of absorbed CH_4 replaced by pure N_2 from the shale reservoir is less. Interestingly, the displacement capacity and displacement efficiency (Figure 16) reach the maximum when the ratio of CO_2 and N_2 is 1:1, with displacement capacity and displacement efficiency up to 2.2 mmol·g^{-1} and 81.5%, respectively. This is because the appropriate amount of CO_2 can replace the absorbed CH_4 from the shale reservoir, and free-state N_2 has the benefit of displacing the desorbed CH_4 from the shale pores. As the proportion of CO_2 increases, more CO_2 will be absorbed on the shale reservoir, which makes it possible to block the shale pores and prevent the desorption of CH_4.

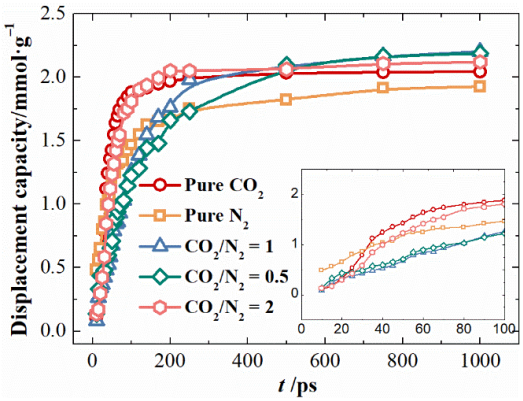

Figure 13. Displacement capacity of CH_4 by gas with different proportions over time.

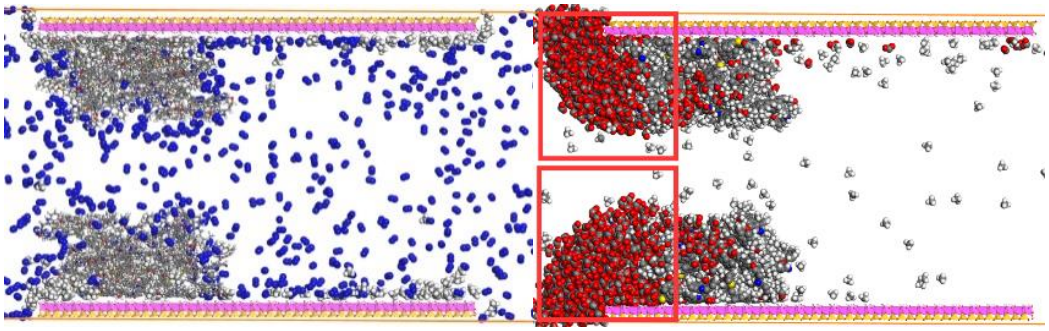

(**a**) N_2 (**b**) CO_2

Figure 14. The simulated snapshots of the displacement process of CH_4 by injection gas: (**a**) N_2; (**b**) CO_2.

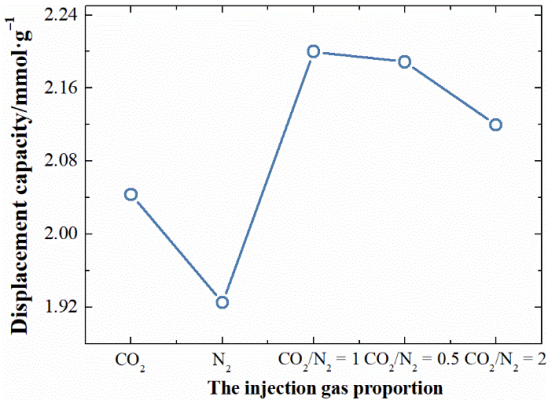

Figure 15. The terminal displacement capacity of CH_4 as a function of the gas proportion.

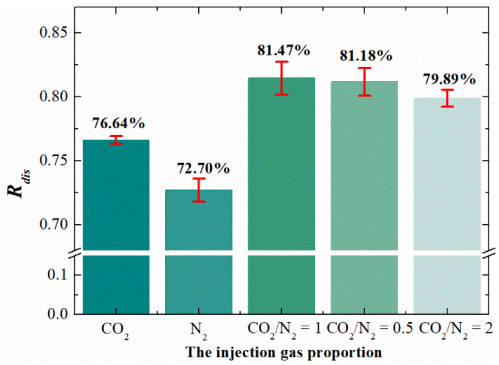

Figure 16. The displacement efficiency of CH_4 as a function of the gas proportion.

3.5. The Influence of Water Content on the Displacement Characteristics

Figure 17 shows the displacement capacity of CH_4 with different water contents over time. It indicates that with the increase in water content, the displacement capacity decreases. When the displacement process reaches a steady-state, the displacement capacity of CH_4 decreases from 2.04 mmol·g^{-1} to 1.68 mmol·g^{-1} as the water content increases from 0 wt.% to 1.6 wt.%. This can be explained as follows: (1) water molecules prevent CO_2 molecules from entering the shale matrix and replacing the absorbed CH_4; (2) the water content can reduce the connectivity of the shale matrix (Figure 18)-that is, with the increase of water content, the free volume and surface area of shale gradually decrease; and (3) the existence of water molecules reduces the amount of pre-adsorbed CH_4 in the shale reservoir (Figure 19). The reason for the low adsorption of CH_4 with high water content can be attributed to the fact that water molecules occupy the adsorption sites of CH_4. Besides, the displacement efficiency of CH_4 decreases as the water content increases, as presented in Figure 20, which means that the water content in the shale reservoir is not conducive to shale exploitation.

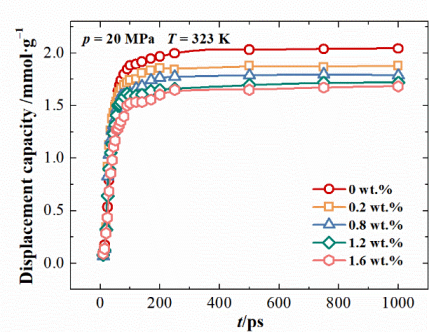

Figure 17. The displacement capacity of CH_4 in the reservoir with different water contents.

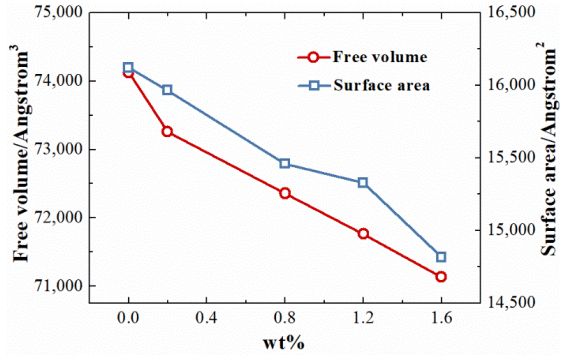

Figure 18. Free volume and surface area of the shale model with different water contents.

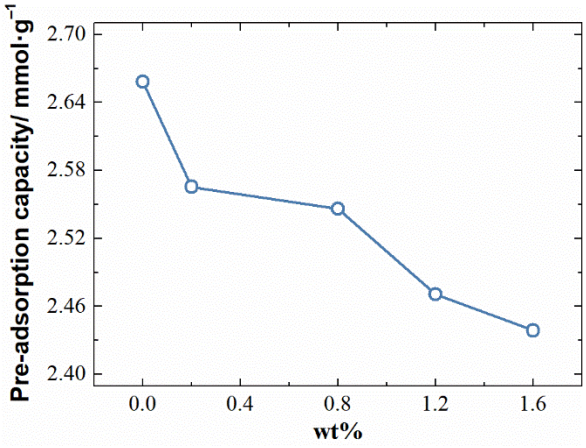

Figure 19. Pre-adsorption capacity of CH_4 in the composite shale reservoir with different water contents.

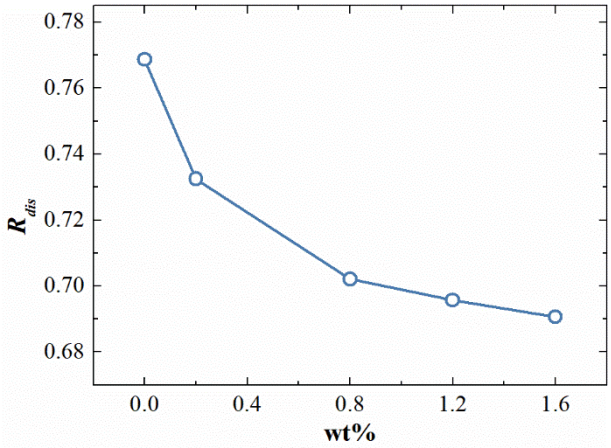

Figure 20. The displacement efficiency of CH_4 in the composite shale reservoir with different water contents.

4. Conclusions

In this paper, the displacement characteristics of CH_4 by CO_2, N_2, and their mixture were investigated by molecular simulations based on a kaolinite–kerogen IID composite shale model. The influence of some factors, including injection pressure, formation temperature, pore size, water content, and gas proportion on the displacement characteristics were examined, and the main results are as follows:

(1) When the injection pressure is smaller than 10 MPa, an effective way to improve the displacement capacity of CH_4 is to increase the injection pressure; the displacement efficiency increased by 44.4% with a pressure increase from 6 MPa to 10 MPa. However, when p > 10 MPa, the growth of the displacement efficiency was not apparent with the further increase of pressure, and the displacement efficiency only increased by 7.0% as the pressure increased from 10 MPa to 20 MPa. Formation temperature was one of the crucial factors affecting displacement efficiency, and as the formation temperature increased, the displacement efficiency increased monotonically.

(2) When the process reached a steady-state, the displacement efficiency increased by 2.6% as the pore size increased from 1 nm to 3 nm. The water content decreased the pre-adsorption capacity and the displacement capacity of CH_4 by decreasing the volume fraction of shale pores.

(3) Compared with N_2, CO_2 showed better displacement capacity on CH_4. The displacement ability of CO_2-N_2 mixed gas was greater than that of CO_2 and N_2 alone, and the optimal gas ratio of CO_2/N_2 at which the displacement efficiency reached the maximum of 81.5% was about 1:1.

In the present study, only the displacement characteristics of CH_4 in a shale reservoir slit with an aperture smaller than 3 nm was investigated. However, the pores of a real shale reservoir may be very different from the present model. Thus, it is necessary to investigate the influence of pore morphology and injection gases on the transport properties of CH_4 in future research.

Author Contributions: Conceptualization, L.G. and N.L.; methodology, Z.-K.G.; software, N.L.; validation, Z.-K.G., B.D., and N.L.; formal analysis, C.-Y.Z.; investigation, Y.Z.; resources, L.G.; data curation, Z.-K.G. and N.L.; writing—original draft preparation, Y.Z.; writing—review and editing, C.-Y.Z. and L.G.; visualization, Y.Z.; supervision, C.-Y.Z.; project administration, L.G.; funding acquisition, C.-Y.Z. and L.G. All authors have read and agreed to the published version of the manuscript.

Funding: This research was funded by the National Natural Science Foundation of China (No. 52006243, No. 51936001, and No. 51676208) and the Fundamental Research Funds for the Central Universities (No.18cx07012a and 20CX06055A).

Data Availability Statement: The authors declare that the data presented in this study are available within the article.

Conflicts of Interest: The authors declare no conflict of interest.

References

1. Hu, Y.; Ma, X.; Li, W.; Wu, W.; Tu, D. Forecasting manufacturing industrial natural gas consumption of China using a novel time-delayed fractional grey model with multiple fractional order. *Comput. Appl. Math.* **2020**, *39*, 263. [CrossRef]
2. Melikoglu, M. Shale gas: Analysis of its role in the global energy market. *Renew. Sustain. Energy Rev.* **2014**, *37*, 460–468. [CrossRef]
3. Ji, L.; Zhang, T.; Milliken, K.; Qu, J.; Zhang, X. Experimental investigation of main controls to methane adsorption in clay-rich rocks. *Appl. Geochem.* **2012**, *27*, 2533–2545. [CrossRef]
4. Shi, J.; Gong, L.; Sun, S.; Huang, Z.; Ding, B.; Yao, J. Competitive adsorption phenomenon in shale gas displacement processes. *RSC Adv.* **2019**, *9*, 25326–25335. [CrossRef]
5. Clarkson, C.R.; Haghshenas, B.; Ghanizadeh, A.; Qanbari, F.; Williams-Kovacs, J.D.; Riazi, N.; Debuhr, C.; Deglint, H.J. Nanopores to megafractures: Current challenges and methods for shale gas reservoir and hydraulic fracture characterization. *J. Nat. Gas Sci. Eng.* **2016**, *31*, 612–657. [CrossRef]
6. Dzombak, D.A. Moving beyond forensic monitoring to understand and manage impacts of hydraulic fracturing for oil and gas development. *Proc. Natl. Acad. Sci. USA* **2018**, *115*, 13145–13147. [CrossRef]
7. Jackson, R.E.; Gorody, A.W.; Mayer, B.; Roy, J.W.; Ryan, M.C.; Van Stempvoort, D.R. Groundwater protection and unconventional gas extraction: The critical need for field-based hydrogeological research. *Groundwater* **2013**, *51*, 488–510. [CrossRef]
8. Wang, L.; Yao, B.; Xie, H.; Winterfeld, P.; Kneafsey, T.; Yin, X. CO_2 injection-induced fracturing in naturally fractured shale rocks. *Energy* **2017**, *139*, 1094–1110. [CrossRef]
9. Du, X.; Gu, M.; Duan, S.; Xian, X. The influences of CO_2 injection pressure on CO_2 dispersion and the mechanism of CO_2–CH_4 displacement in shale. *J. Energy Resour. Technol. Trans. ASME* **2018**, *140*, 012907. [CrossRef]
10. Godec, M.; Koperna, G.; Petrusak, R.; Oudinot, A. Enhanced gas recovery and CO_2 storage in gas shales: A summary review of its status and potential. *Energy Procedia* **2014**, *63*, 5849–5857. [CrossRef]
11. Huo, P.; Zhang, D.; Yang, Z.; Li, W.; Zhang, J.; Jia, S. CO_2 geological sequestration: Displacement behavior of shale gas methane by carbon dioxide injection. *Int. J. Greenh. Gas Control* **2017**, *66*, 48–59. [CrossRef]
12. Akbarzadeh, H.; Abbaspour, M.; Salemi, S.; Akbari, M. Injection of mixture of shale gases in a nanoscale pore of graphite and their displacement by CO_2/N_2 gases using molecular dynamics study. *J. Mol. Liq.* **2017**, *248*, 439–446. [CrossRef]
13. Hou, P.; Gao, F.; Gao, Y.; Yang, Y.; Cai, C. Effect of pore pressure distribution on fracture behavior of sandstone in nitrogen fracturing. *Energy Explor. Exploit.* **2017**, *35*, 609–626. [CrossRef]
14. Seomoon, H.; Lee, M.; Sung, W. Analysis of methane recovery through CO_2–N_2 mixed gas injection considering gas diffusion phenomenon in coal seam. *Energy Explor. Exploit.* **2016**, *34*, 661–675. [CrossRef]
15. Lyu, Q.; Long, X.; Ranjith, P.G.; Tan, J.; Kang, Y.; Wang, Z. Experimental investigation on the mechanical properties of a low-clay shale with different adsorption times in sub-/super-critical CO_2. *Energy* **2018**, *147*, 1288–1298. [CrossRef]
16. Du, F.; Nojabaei, B. A review of gas injection in shale reservoirs: Enhanced oil/gas recovery approaches and greenhouse gas control. *Energies* **2019**, *12*, 2355. [CrossRef]
17. Liu, J.; Yao, Y.; Liu, D.; Elsworth, D. Experimental evaluation of CO_2 enhanced recovery of adsorbed-gas from shale. *Int. J. Coal Geol.* **2017**, *179*, 211–218. [CrossRef]
18. Du, X.D.; Gu, M.; Duan, S.; Xian, X.-F. Investigation of CO_2-CH_4 displacement and transport in shale for enhanced shale gas recovery and CO_2 sequestration. *J. Energy Resour. Technol. Trans. ASME* **2017**, *139*, 012909. [CrossRef]

19. Du, X.; Gu, M.; Liu, Z.; Zhao, Y.; Sun, F.; Wu, T. Enhanced shale gas recovery by the injections of CO_2, N_2 and CO_2/N_2 mixture gases. *Energy Fuels* **2019**, *33*, 5091–5101. [CrossRef]
20. Chen, T.; Feng, X.-T.; Pan, Z. Experimental study on kinetic swelling of organic-rich shale in CO_2, CH_4 and N_2. *J. Nat. Gas Sci. Eng.* **2018**, *55*, 406–417. [CrossRef]
21. Wang, L.; Yao, B.; Cha, M.; Alqahtani, N.B.; Patterson, T.W.; Kneafsey, T.J. Waterless fracturing technologies for unconventional reservoirs opportunities for liquid nitrogen. *J. Nat. Gas Sci. Eng.* **2016**, *35*, 160–174. [CrossRef]
22. Wang, H.; Qu, Z.; Yin, Y.; Bai, J.; Yu, B. Review of molecular simulation method for gas adsorption/desorption and diffusion in shale matrix. *J. Therm. Sci.* **2019**, *28*, 1–16. [CrossRef]
23. Sun, H.; Zhao, H.; Qi, N.; Li, Y. Molecular insights into the enhanced shale gas recovery by carbon dioxide in kerogen slit nanopores. *J. Phys. Chem. C* **2017**, *121*, 10233–10241. [CrossRef]
24. Liu, X.-Q.; Xue, Y.; Tian, Z.-Y.; Mo, J.-J.; Qiu, N.-X.; Chu, W. Adsorption of CH_4 on nitrogen- and boron-containing carbon models of coal predicted by density-functional theory. *Appl. Surf. Sci.* **2013**, *285*, 190–197. [CrossRef]
25. Zhou, W.; Zhang, Z.; Wang, H.; Yan, Y.; Liu, X. Molecular insights into competitive adsorption of CO_2/CH_4 mixture in shale nanopores. *RSC Adv.* **2018**, *8*, 33939–33946. [CrossRef]
26. Zhang, B.; Kang, J.; Kang, T. Monte Carlo simulations of methane adsorption on kaolinite as a function of pore size. *J. Nat. Gas Sci. Eng.* **2018**, *49*, 410–416. [CrossRef]
27. Xiong, J.; Liu, K.; Liu, X.; Liang, L.; Zeng, Q. Molecular simulation of methane adsorption in slit-like quartz pores. *RSC Adv.* **2016**, *6*, 110808–110819. [CrossRef]
28. Sun, H.; Zhao, H.; Qi, N.; Qi, X.; Zhang, K.; Li, Y. Molecular insight into the micro-behaviors of CH_4 and CO_2 in montmorillonite slit-nanopores. *Mol. Simul.* **2017**, *43*, 1004–1011. [CrossRef]
29. Lin, K.; Yuan, Q.; Zhao, Y.-P.; Cheng, C. Which is the most efficient candidate for the recovery of confined methane: Water, carbon dioxide or nitrogen? *Extrem. Mech. Lett.* **2016**, *9*, 127–138. [CrossRef]
30. Zhang, H.; Cao, D. Molecular simulation of displacement of shale gas by carbon dioxide at different geological depths. *Chem. Eng. Sci.* **2016**, *156*, 121–127. [CrossRef]
31. Young, R.; Hewat, A. Verification of the triclinic crystal structure of kaolinite. *Clays Clay Miner.* **1988**, *36*, 225–232. [CrossRef]
32. Ungerer, P.; Collell, J.; Yiannourakou, M. Molecular modeling of the volumetric and thermodynamic properties of kerogen: Influence of organic type and maturity. *Energy Fuels* **2015**, *29*, 91–105. [CrossRef]
33. Okiongbo, K.; Aplin, A.; Larter, S. Changes in type II kerogen density as a function of maturity: Evidence from the kimmeridge clay formation. *Energy Fuels* **2005**, *19*, 2495–2499. [CrossRef]
34. Perez, F.; Devegowda, D. Estimation of adsorbed-phase density of methane in realistic overmature kerogen models using molecular simulations for accurate gas in place calculations. *J. Nat. Gas Sci. Eng.* **2017**, *46*, 865–872. [CrossRef]